



OPEN ACCESS

EDITED BY

Wenwu Xu,
San Diego State University, United States

REVIEWED BY

Chao Wang,
Ansys, United States
Dunja Peric,
Kansas State University, United States

*CORRESPONDENCE

Rongzhou Yang,
✉ Rongzhouy@outlook.com
Ying Xu,
✉ yxu@aust.edu.cn

RECEIVED 01 March 2024

ACCEPTED 30 May 2024

PUBLISHED 19 June 2024

CITATION

Yang R, Xu Y, Yu M, Ge J, An Q and Ma P
(2024), Rock-like material under large
diameter SHPB dynamic splitting tension:
meso-damage mechanical behavior and
stress wave propagation model.
Front. Mater. 11:1394233.
doi: 10.3389/fmats.2024.1394233

COPYRIGHT

© 2024 Yang, Xu, Yu, Ge, An and Ma. This is an
open-access article distributed under the
terms of the [Creative Commons Attribution
License \(CC BY\)](https://creativecommons.org/licenses/by/4.0/). The use, distribution or
reproduction in other forums is permitted,
provided the original author(s) and the
copyright owner(s) are credited and that the
original publication in this journal is cited, in
accordance with accepted academic practice.
No use, distribution or reproduction is
permitted which does not comply with
these terms.

Rock-like material under large diameter SHPB dynamic splitting tension: meso-damage mechanical behavior and stress wave propagation model

Rongzhou Yang^{1,2,3*}, Ying Xu^{1,3*}, Meilu Yu³, Jinjin Ge¹, Qi An¹
and Pengying Ma¹

¹School of Civil Engineering and Architecture, Anhui University of Science and Technology, Huainan, China, ²Anhui Hongchang New Materials Co., Ltd., Huaibei, China, ³State Key Laboratory of Mining Response and Disaster Prevention and Control in Deep Coal Mines, Anhui University of Science and Technology, Huainan, China

The mechanical behavior of splitting tensile damage and the law of stress wave propagation of rock-like materials (RLM) are of great significance to further reveal the dynamic disaster mechanism of the deep rock mass. The meso-damage mechanical behavior and stress wave propagation characteristics of RLM disks under impact splitting were studied by using a large diameter split Hopkinson pressure bar (SHPB). In terms of dynamic damage, the splitting tensile stress-compression strain curves of RLM disks obviously showed three stages of mechanical behavior evolution: initial elastic-plastic deformation, pre-peak plastic damage, and post-peak brittle fracture failure. The macro-damage of RLM disks increased with the increase of strain rate. The meso-tensile fracture was the result of both the initial meso-damage and the impact splitting meso-damage. The dynamic splitting damage variable defined based on the damage fracture energy can accurately describe the damage evolution characteristics of impact splitting on RLM disks. In the aspect of stress wave propagation, the peak value of transmission stress showed an advanced effect with the increase of incident stress wave. In the early stage (0–50 μ s), the transmission stress wave ratio (σ_T/σ_I) increased with the increase of strain rate, while in the later stage (82–200 μ s), the transmission stress wave ratio (σ_T/σ_I) decreased with the increase of strain rate. The stress wave propagation law in the process of impact splitting on RLM disks was clearly revealed based on the stress wave propagation model established by the one-dimensional elastic stress wave theory. Finally, the dynamic mechanical mechanism of splitting damage and fracture of RLM disks under different strain rates was discussed deeply.

KEYWORDS

rock-like material (RLM), dynamic splitting tension, strain rate effect, dynamic mechanical mechanism, stress wave propagation

1 Introduction

With the increasing buried depth of energy development and engineering construction, the geological environment becomes more complex, so the phenomenon of dynamic disasters becomes more prominent, which has become a major problem hindering deep

energy development and engineering construction (Fairhurst, 2017; Chen et al., 2019; Li et al., 2020). To solve this problem fundamentally, it is necessary to truly reflect the actual state of deep-buried rock mass through a series of scientific model tests, to get more practical results (Gao et al., 2018; Xie et al., 2022; Zhu et al., 2022). Therefore, in addition to numerical simulation analysis (Guo et al., 2022; Yang et al., 2022) and on-site dynamic monitoring (Ma et al., 2015; Xue et al., 2021), the indoor physical model test is also a very important way to study the stability of deep surrounding rock (Zuo et al., 2011; Li et al., 2016; Liu et al., 2021). However, considering that it is difficult to obtain deep-buried big bulk intact rock mass and difficult to process complex rock mass model, many scholars often use “cement mortar materials” which are similar to real rock materials as “rock similar materials (RLM)” to carry out a series of scientific experiments (Zhang et al., 2017; Zheng et al., 2021; Li P. et al., 2023). Therefore, “cement mortar type RLM” plays an important role in the scientific research on the mechanism and prevention of deep rock dynamic disasters.

The rock with frequent dynamic disasters is generally quasi-elastic-brittle material. Because the tensile strength of rock is significantly lower than its compressive strength, rock is more prone to tensile failure under dynamic loads such as blasting and excavation (Xue et al., 2013). Therefore, the tensile mechanical properties of rock become one of the main mechanical factors that determine the failure of rock. Even in the process of compression, the failure form of rock is often the overall failure caused by the tensile failure of its internal micro-cracks, which inevitably contains a profound tensile fracture mechanics mechanism (Guo and Man, 2022). Many engineering phenomena and scientific studies (Deng et al., 2019; Zhai et al., 2020; Hu et al., 2021; Zhang et al., 2021; Wang J. et al., 2022) have shown that dynamic splitting tensile failure is an important form of damage and fracture of deep surrounding rock (such as zonal fracture of surrounding rock (Zuo et al., 2011)). As shown in Figure 1 (Wang Z. et al., 2022), usually, before excavation, the rock mass element is in a three-dimensional initial stress state ($\sigma_1, \sigma_2, \sigma_3$). In the process of excavation, the stress redistribution occurs in the stress state of the rock mass element, which leads to the increase of σ_1 and the decrease of σ_3 . The stress state of the rock mass element gradually changes from the three-dimensional stress state ($\sigma_3 > 0$) to the two-dimensional stress state ($\sigma_3 = 0$). The damage state of the rock mass element changes from the intact state to the splitting plate state. If the stress σ_1 exceeds the uniaxial compressive strength (The red dot in Figure 1 is the uniaxial compressive strength of the rock.) of the rock and stores a large amount of elastic strain energy in the rock mass element, the elastic strain energy will be released in a very short time, and the rock mass element will show nonlinear dynamic characteristics, that is, the surrounding rock of the deep roadway is more prone to buckling rockburst due to splitting damage. Therefore, dynamic splitting tensile failure is a direct factor leading to further buckling dynamic instability of surrounding rock. To prevent catastrophic accidents caused by rock failure and instability in geotechnical engineering, it is necessary to study the dynamic tensile mechanical properties of rock and its inherent mechanism (Xue et al., 2013). Therefore, the accurate acquisition of rock dynamic tensile mechanical properties and the profound revelation of fracture mechanism are very important to scientifically and reasonably use rock dynamic parameters and mechanical

mechanisms to analyze geotechnical engineering and effectively solve practical engineering problems. What needs to be paid more attention to is that to accurately verify and further improve the coincidence degree of physical and mechanical properties and damage mechanism between RLM and real rock material, when using RLM instead of real rock material as the research object, it is equally important to accurately obtain the dynamic tensile mechanical properties of RLM and reveal its fracture mechanism.

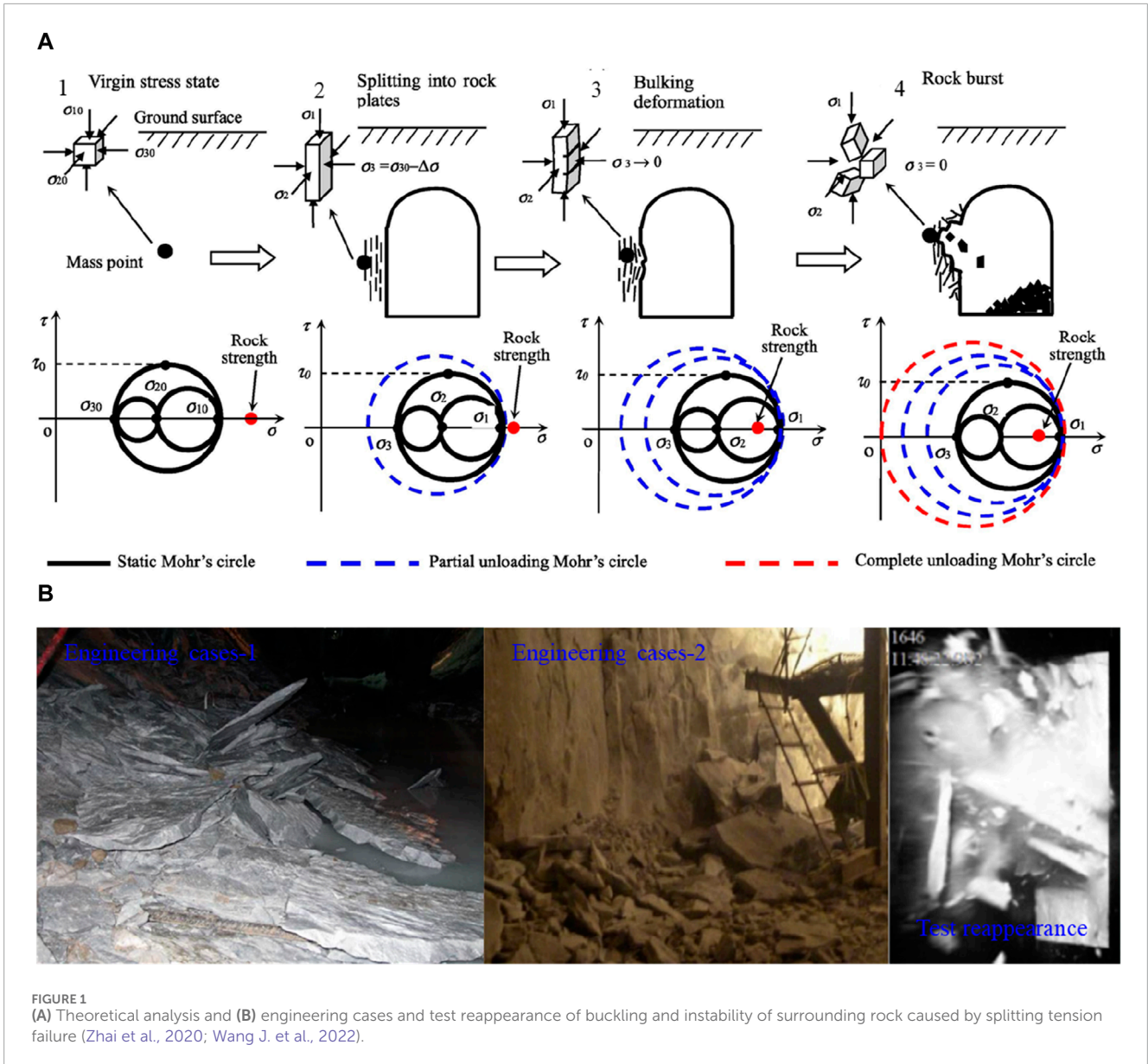
Split Hopkinson pressure bar (SHPB) is a widely used and reliable scientific test system for studying the dynamic characteristics of rock materials (Wang et al., 2009; Xia and Yao, 2015; Han et al., 2022). According to the dynamic tensile strength test method recommended by the International Society for Rock Mechanics (ISRM), the dynamic splitting tensile test of rock Brazilian disk is carried out by using the SHPB dynamic loading system, which has become an efficient and simple scientific test method to study the dynamic tensile properties of rock (Wang et al., 2009; Xia and Yao, 2015; Han et al., 2022). The related literature (Xia and Yao, 2015; Xia et al., 2019; Xia et al., 2021) systematically summarized the latest research results of rock dynamics, with emphasis on the testing equipment, testing principle, test methods, and test results of rock under dynamic tension. The variation law, mutual feedback mechanism, and damage mechanism of dynamic tensile mechanical characteristics for deep rocks were further studied and discussed (Guo and Man, 2022). However, the mechanical behavior and stress wave propagation characteristics of large diameter SHPB impact splitting tensile damage for RLM disk specimens have not been fully and deeply studied, and the effects of stress wave propagation on the dynamic tensile mechanical properties and dynamic mechanical damage mechanism of RLM should also be fully considered.

In view of the shortcomings of the above research, and based on the previous research work (Yang et al., 2023), aiming at a kind of cement mortar type RLM of sandstone, the meso-damage mechanical behavior and one-dimensional elastic stress wave propagation characteristics of RLM disk specimens under large diameter SHPB impact splitting test were studied, and the dynamic mechanical mechanism of splitting damage and fracture of RLM disks under different strain rates was further discussed. The research results can provide some reference for further promoting the effective application of RLM in the scientific research of dynamic disaster mechanisms and prevention and control of deep rock mechanics.

2 Materials and methodology

2.1 Preparation method of RLM disk specimen

According to the research of related literature (Le et al., 2019; Yang et al., 2023), aiming at the physical and mechanical characteristics of fine sandstone, the RLM used in the test was cement mortar material. The mixed water was laboratory tap water, the cementitious material was 42.5-grade ordinary Portland cement, and the fine aggregate was natural fine river sand. The large diameter RLM disk specimens with the size of $\Phi 70 \text{ mm} \times h$



35 mm were prepared by pouring, and the impact splitting test was carried out after the standard curing was completed. The specific preparation and test process of the RLM disk specimens is shown in Figure 2.

2.2 Test equipment and mechanical calculation method

2.2.1 Static splitting test

Based on the Brazilian splitting principle, the static splitting test of RLM disk specimens was carried out by using the YAW-300 static load test system. The test was carried out by controlling the displacement. The schematic diagram of the static load test system and the test results are shown in Figure 3. It can be seen from Figure 3 that the splitting tensile stress-compression strain curve of RLM disk under static load

mainly showed two evolution stages: pre-peak elastic-plastic deformation and post-peak brittle fracture failure. Accordingly, the input energy-compression strain curve mainly showed two evolution stages: pre-peak nonlinear growth and post-peak linear growth.

2.2.2 Dynamic splitting test

Based on the Brazilian splitting principle, the impact splitting test of RLM disk specimens was carried out by using variable cross-section large diameter SHPB test system with Φ 74 mm. The schematic diagram of the SHPB test system is shown in Figure 4A. The density (ρ) of bars in the SHPB test system is 7.8 g/cm³.

The compression strain rate ($\dot{\epsilon}$), compression strain (ϵ), and splitting tensile stress (σ_{st}) of RLM disk specimens under SHPB test can be calculated by two-wave method Eq. 1 (Ai et al., 2019; Li X. et al., 2023).

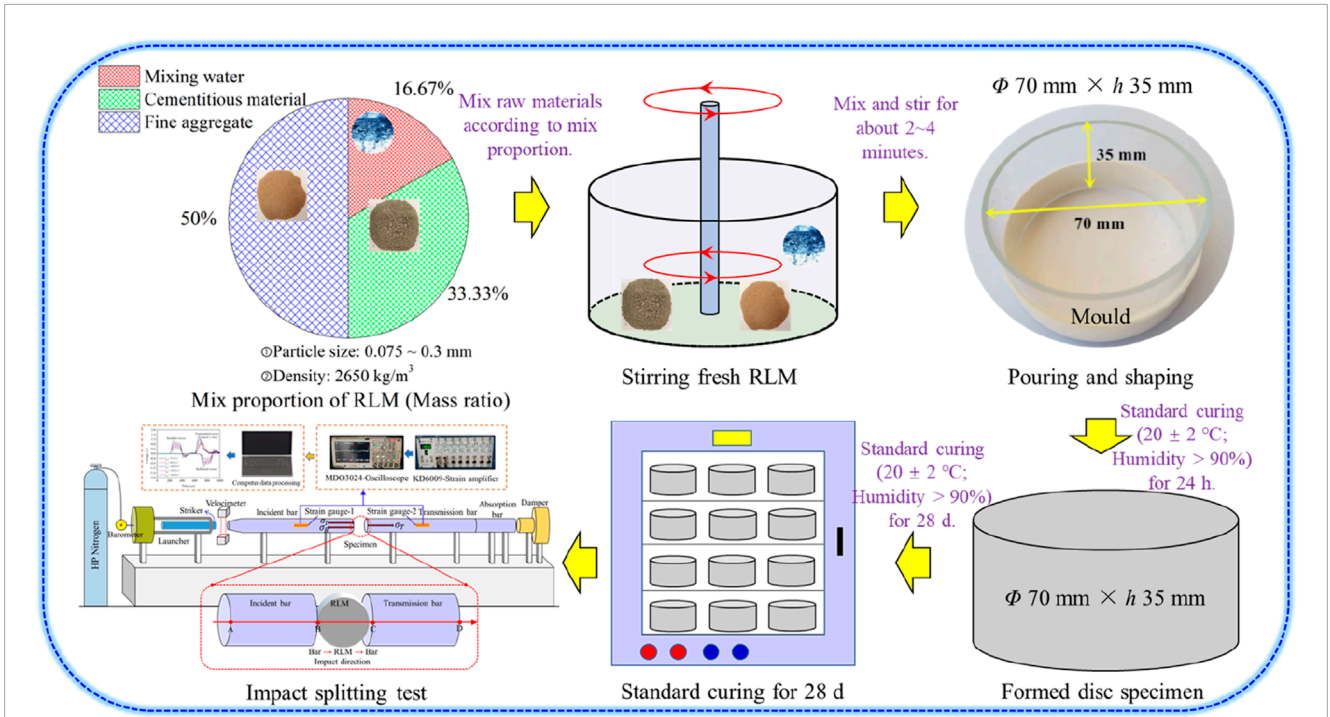


FIGURE 2 Preparation process and impact splitting tests of RLM disk specimens.

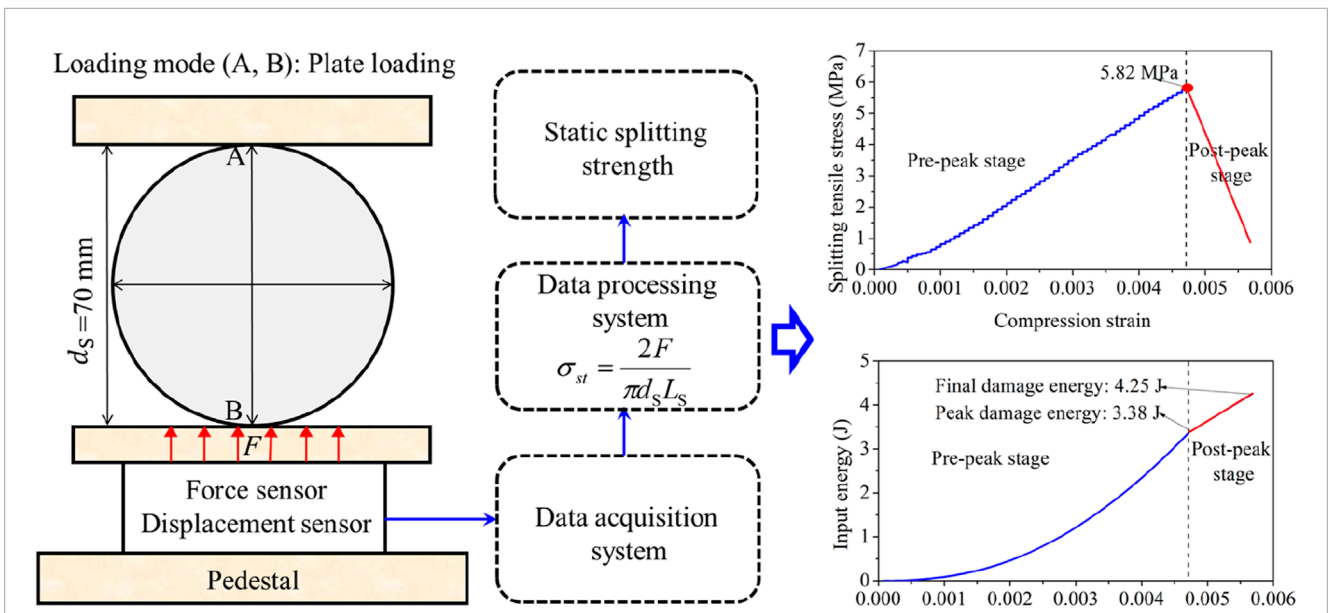


FIGURE 3 Schematic diagram of static load test system and test results.

$$\begin{cases} \dot{\varepsilon}(t) = \frac{2C}{Ed_S} [\sigma_I(t) - \sigma_T(t)] \\ \varepsilon(t) = \frac{2C}{Ed_S} \int_0^t [\sigma_I(t) - \sigma_T(t)] dt \\ \sigma_{st}(t) = \frac{2A}{\pi d_S L_S} \sigma_T(t) \end{cases} \quad (1)$$

where: E is the elastic modulus of the compression bars (210 GPa); A is the cross-sectional area of the compression bars; C is the wave velocity of the compression bars (5190 m/s); L_S is the initial length of the specimen; d_S is the initial diameter of the specimen; σ_I is the incident stress wave in the compression bar;

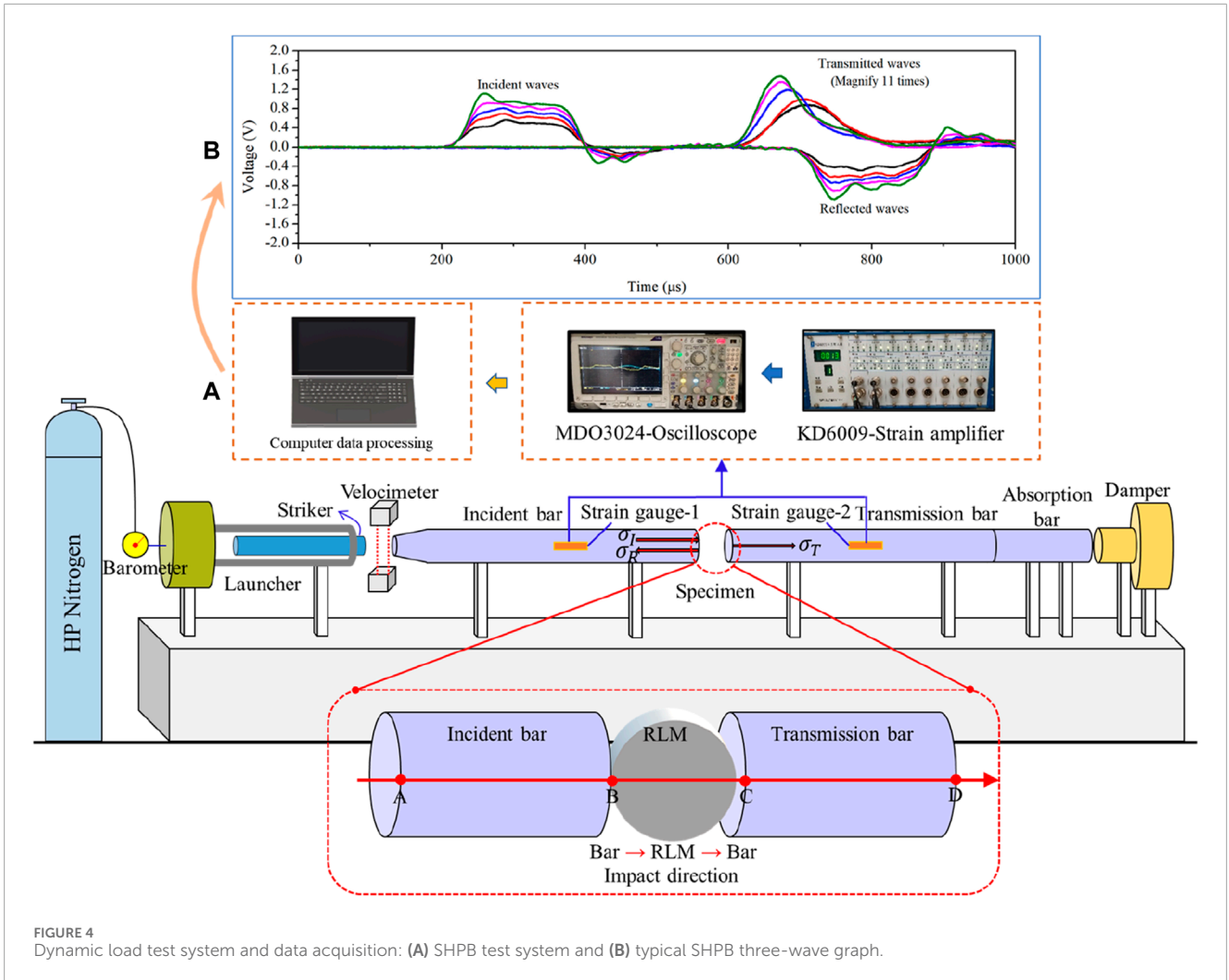


FIGURE 4 Dynamic load test system and data acquisition: (A) SHPB test system and (B) typical SHPB three-wave graph.

σ_T is the transmitted stress wave in the compression bar. The typical SHPB three-wave graph collected in the experiment is shown in Figure 4B.

3 Results and analysis

3.1 Stress-strain curves and meso-damage fracture characteristics

The stress-strain curves and meso-damage fracture characteristics of RLM disks under impact splitting are shown in Figure 5. As can be seen in Figure 5A, the splitting tensile stress-compression strain curves (hereinafter referred to as stress-strain curves) of RLM disks obviously showed three stages of mechanical behavior evolution: initial elastic-plastic deformation, pre-peak plastic damage and post-peak brittle fracture failure. With the increase of strain rate, the deformation modulus, peak stress, and ultimate strain of RLM disks increased continuously, showing an obvious strain rate effect (Yang et al., 2023). The increase of strain rate also led to the increase of macro-damage of RLM disks. Compared with the previous research work (Yang et al., 2023), the

large diameter RLM disk specimens do not show obvious post-peak stress residual phenomenon. According to meso-damage mechanics, under external load, the damage of the material starts from the initial meso-damage, which determines the meso-mechanical properties of the material and ultimately affects the macroscopic mechanical properties of the material. This means that rock damage is the result of the synergistic action of multi-scale structures (Toi and Kiyosue, 1995; Yuan et al., 2013; Ren et al., 2023). As can be seen in Figure 5B, there were many pores and other initial meso-damage on the meso-tensile fracture surfaces of RLM disks, which was similar to the initial pore structure of natural rock materials (Yang et al., 2023). The above further indicated that the tensile fracture of RLM disks at the meso-level is the result of both the initial meso-damage and the impact splitting meso-damage.

3.2 Energy damage and strength performance

Combined with the two-wave method Eq. 1, the incident energy (W_I), reflection energy (W_R), transmission energy (W_T), and

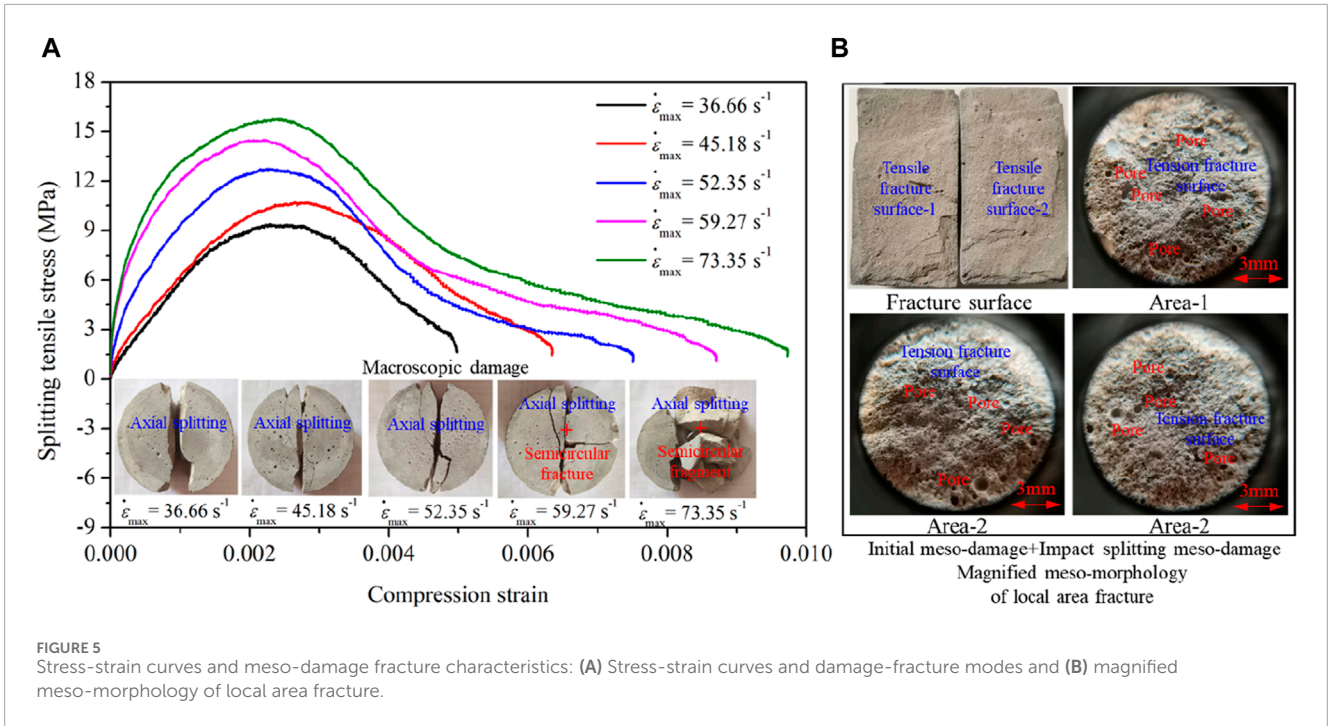


FIGURE 5 Stress-strain curves and meso-damage fracture characteristics: (A) Stress-strain curves and damage-fracture modes and (B) magnified meso-morphology of local area fracture.

damage energy (W_D) in SHPB test can be calculated by Eq. 2 (Wu et al., 2019; Chen et al., 2022).

$$\begin{cases} W_I(t) = \frac{AC}{E} \int_0^t \sigma_I^2(t) dt \\ W_R(t) = \frac{AC}{E} \int_0^t [\sigma_I(t) - \sigma_T(t)]^2 dt \\ W_T(t) = \frac{AC}{E} \int_0^t \sigma_T^2(t) dt \\ W_D(t) = W_I(t) - W_R(t) - W_T(t) \end{cases} \quad (2)$$

According to the energy driving theory, energy is the essential driving force to drive the damage of materials (Wang et al., 2023). Therefore, the damage fracture energy can well reflect the damage evolution state of materials.

According to the two-wave method energy calculation Eq. 2, based on the damage fracture energy, the two-wave method calculation Eq. 3 of dynamic damage variable can be further obtained (Yang et al., 2023):

$$D(t) = \frac{2AC \int_0^t [\sigma_I(t)\sigma_T(t) - \sigma_T^2(t)] dt}{EW_{D,max}} \quad (3)$$

where: D is the dynamic splitting damage variable of RLM disks under impact splitting; $W_{D,max}$ is the maximum damage fracture energy of RLM disks under impact splitting in this test.

According to Eq. 3, the dynamic splitting damage evolution curves of RLM disks under impact splitting can be obtained (Figure 6A). As can be seen in Figure 6, the dynamic splitting damage variables of RLM disks increased with the increase of strain, and the maximum dynamic splitting damage variables and peak stress increased linearly with the increase of strain rate, which showed that the dynamic splitting strength of RLM under impact splitting depended on the degree of dynamic splitting damage.

3.3 Stress-strain curves and energy damage-strain curves

The comparative analysis of the evolution characteristics between the stress-strain curves and the energy damage-strain curves of RLM disks under impact splitting is shown in Figure 7. As can be seen in Figure 7, the time for the curves to reach the pre-peak key point b and the peak stress point c decreased with the increase of strain rate, showing the advance effect of stress key points and damage key points.

- (1) In the initial elastic-plastic deformation stage (ab): The energy damage value is at a very low level, and the impact driving energy input into the RLM disk is mainly transformed into elastic strain energy. The slight damage at the loading end occurs mainly due to the stress concentration at the loading end, and there is no substantial structural damage, and the stress increases obviously.
- (2) In the pre-peak plastic damage stage (bc): The energy damage value is at a high level, and the impact driving energy input into the RLM disk is mainly transformed into elastic strain energy and plastic strain energy. The RLM disk mainly occurs the initial crack damage at the center and further increases the damage at the loading end, which leads to substantial structural damage and weakening stress growth capacity.
- (3) In the post-peak fracture failure stage (cf): The energy damage value is at a very high level, and the impact driving energy input into the RLM disk is mainly transformed into plastic strain energy. The RLM disk mainly occurs splitting tensile fracture caused by the axial expansion of the central initiation damage, and the loading end damage further increases, even semicircle bending fracture occurs, which leads to serious structural damage and reduced stress.

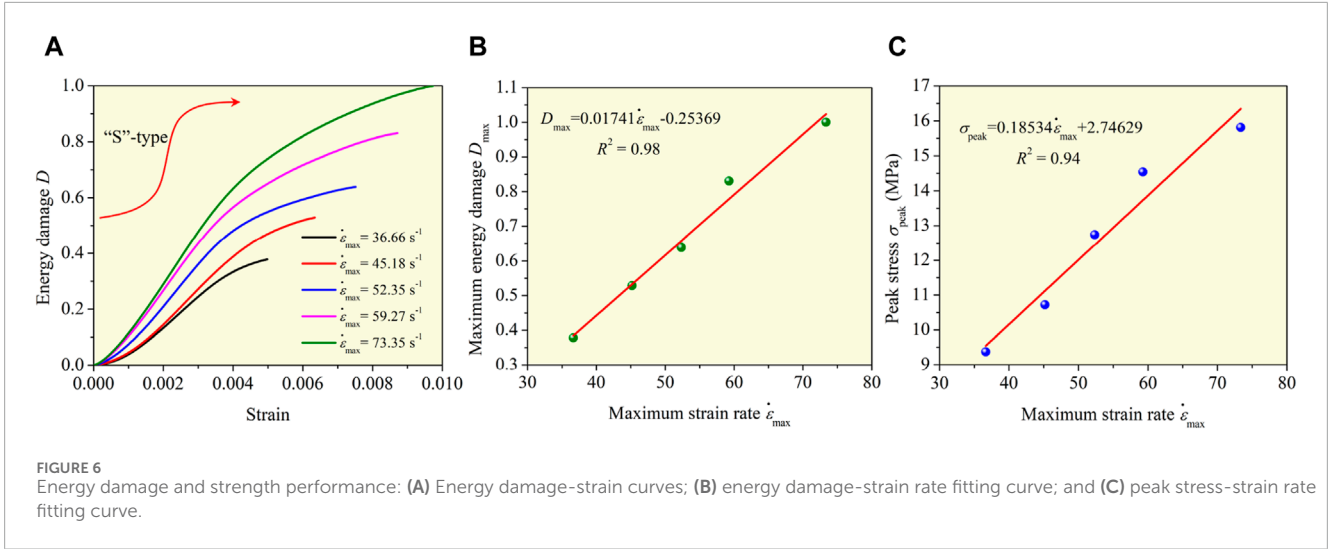


FIGURE 6 Energy damage and strength performance: (A) Energy damage-strain curves; (B) energy damage-strain rate fitting curve; and (C) peak stress-strain rate fitting curve.

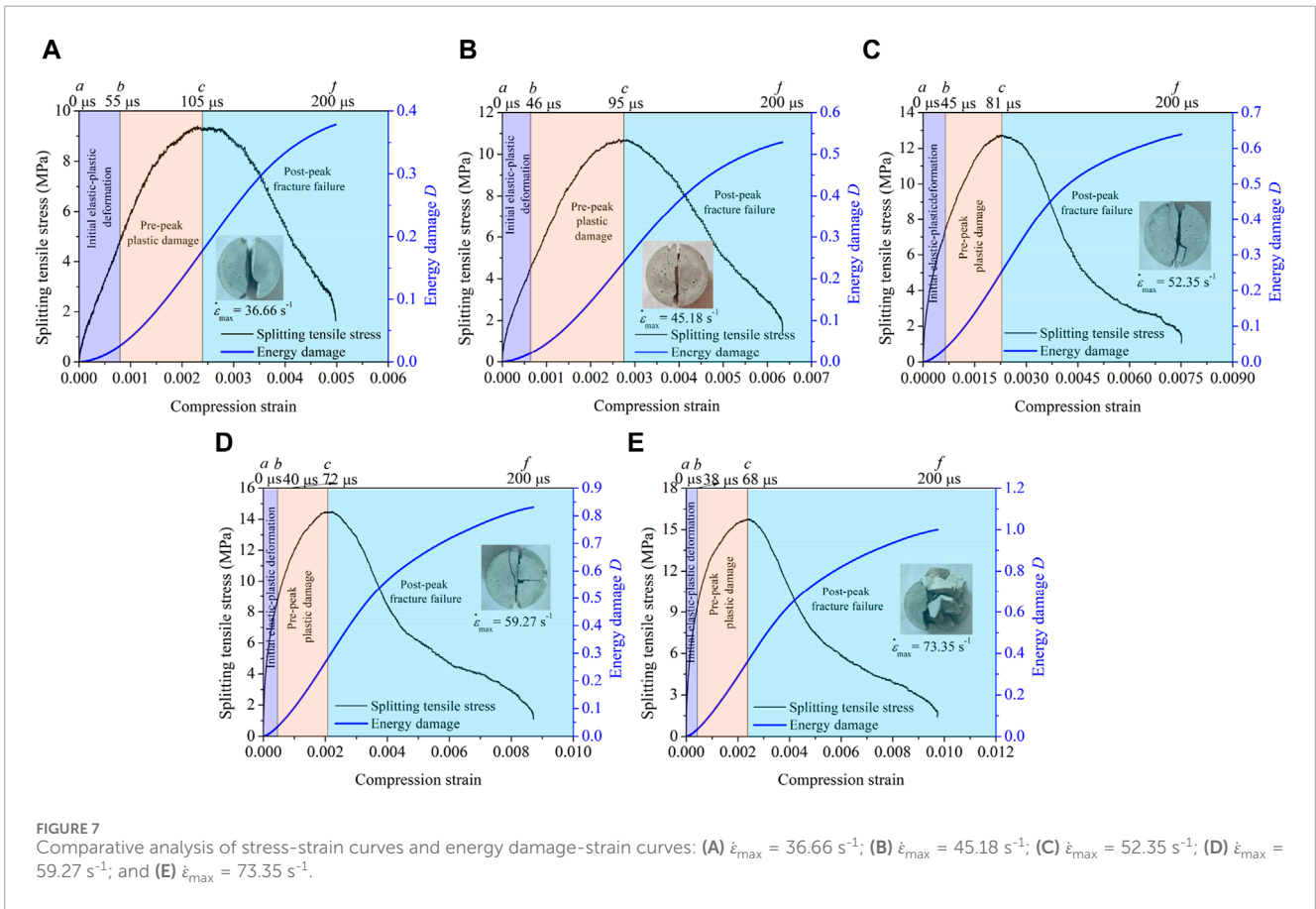


FIGURE 7 Comparative analysis of stress-strain curves and energy damage-strain curves: (A) $\dot{\epsilon}_{max} = 36.66 \text{ s}^{-1}$; (B) $\dot{\epsilon}_{max} = 45.18 \text{ s}^{-1}$; (C) $\dot{\epsilon}_{max} = 52.35 \text{ s}^{-1}$; (D) $\dot{\epsilon}_{max} = 59.27 \text{ s}^{-1}$; and (E) $\dot{\epsilon}_{max} = 73.35 \text{ s}^{-1}$.

3.4 Stress rate-time curves and energy damage rate-time curves

The comparative analysis of the evolution characteristics of stress rate-time curves and energy damage rate-time curves of RLM disks under impact splitting is shown in Figure 8. As can be seen in Figure 8, the stress rate-time curves were approximately centrally symmetrical at the peak stress point c , and the time for the curves to

reach the post-peak key points d and e decreased with the increase of strain rate, which also showed the advance effect of stress rate key points and damage rate key points.

- (1) In the initial elastic-plastic deformation stage (ab): The stress rate and energy damage rate increased synchronously with time, but the difference was that the stress rate increased approximately with a "positive linear" trend, while the energy

damage rate mainly showed an increasing trend of “slow first and then fast”. The stress rate was greater than zero and reached its maximum at point *b*. The above results showed that the stress enhancement mechanism and energy damage mechanism are enhanced simultaneously, but the stress enhancement mechanism is larger than the energy damage mechanism, which makes the stress enhancement mechanism play a dominant role.

- (2) In the pre-peak plastic damage stage (*bc*): The stress rate began to decrease with time, and approximately decreased with a “negative linear” trend, while the energy damage rate increased with a “positive linear” trend, and reached the maximum value near the left side of the peak stress point *c*. The stress rate was greater than zero and reached zero at the peak stress point *c*. The above results showed that the stress enhancement mechanism is weakened and the energy damage mechanism is enhanced, but the stress enhancement mechanism is still larger than the energy damage mechanism, so that the stress enhancement mechanism still plays a dominant role.
- (3) In the post-peak fracture failure stage (*cd*): The stress rate and energy damage rate decreased synchronously with time in a “negative linear” trend. The stress rate was less than zero and reached a minimum at point *d*. The above results showed that the stress enhancement mechanism and energy damage mechanism are weakened simultaneously, but the stress enhancement mechanism is smaller than the energy damage mechanism, which makes the energy damage mechanism play a dominant role.
- (4) In the post-peak fracture failure stage (*de*): The stress rate increased with time with a “positive linear” trend, and the energy damage rate decreased with time with a negative linear trend. The above results showed that the stress enhancement mechanism is enhanced and the energy damage mechanism is weakened, but the stress enhancement mechanism is still smaller than the energy damage mechanism, so the energy damage mechanism still plays a dominant role.
- (5) In the post-peak fracture failure stage (*ef*): The stress rate showed a “horizontal fluctuation” phenomenon with time, and the energy damage rate decreased with a “negative linear” trend with time. The above results showed that the stress enhancement mechanism is in a stable state, and the energy damage mechanism continues to weaken, but the stress enhancement mechanism is still smaller than the energy damage mechanism, which makes the energy damage mechanism still play a dominant role.

3.5 Evolution characteristics of dynamic energy ratio-time curves

The evolution characteristics of the dynamic energy ratio-time curves of RLM disks under impact splitting are shown in Figure 9. As can be seen from Figure 9, the dynamic energy ratio-time curves of RLM disks under impact splitting mainly showed two different evolution stages, namely, the early stage and the later stage, with the curve intersection area at 110 μs as the boundary point. In general, the reflected energy ratio mainly showed a trend of “rapid growth

first, then fluctuation and stability”, and the transmitted energy ratio and damage energy ratio mainly showed a trend of “rapid decrease first, then fluctuation and stability”. Locally, in the early stage (0–110 μs), the reflected energy ratio decreased with the increase of strain rate, while the transmitted energy ratio and damage energy ratio increased with the increase of strain rate, which indicated that the increase of strain rate can promote the transmission of stress waves in the early stage. In the later stage (110–200 μs), the reflected energy ratio increased with the increase of strain rate, while the transmitted energy ratio and damage energy ratio decreased with the increase of strain rate, which indicated that the increase of strain rate can promote the reflection of stress waves in the later stage. The above phenomena and results can reflect that the impact damage degree of the RLM disks in the early stage is less than that in the later stage.

4 Stress wave propagation model

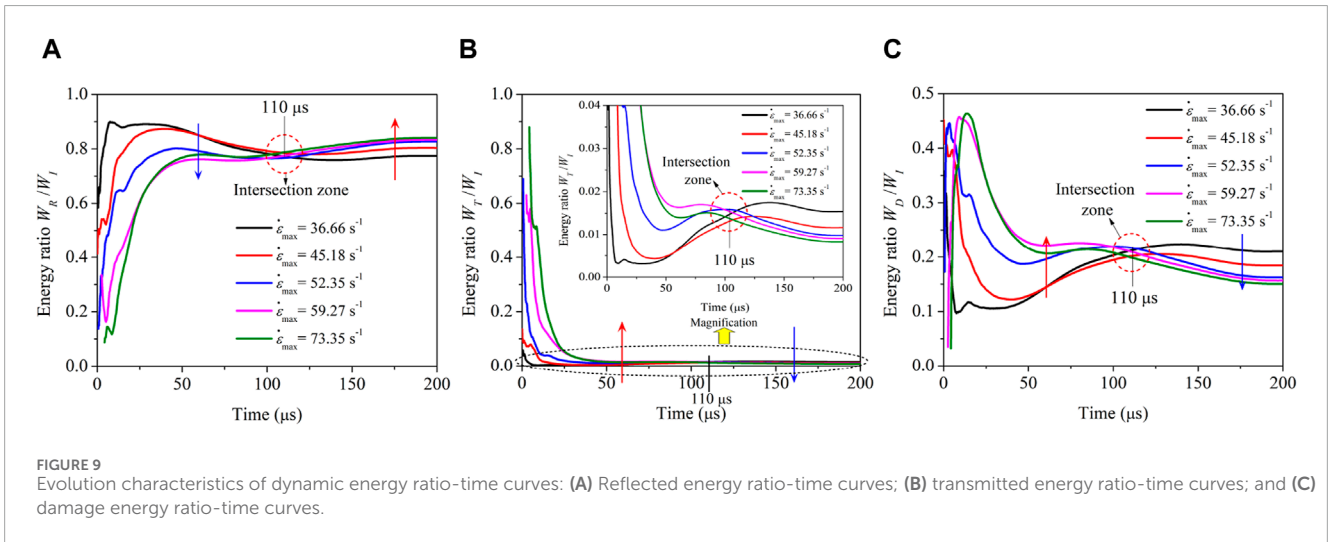
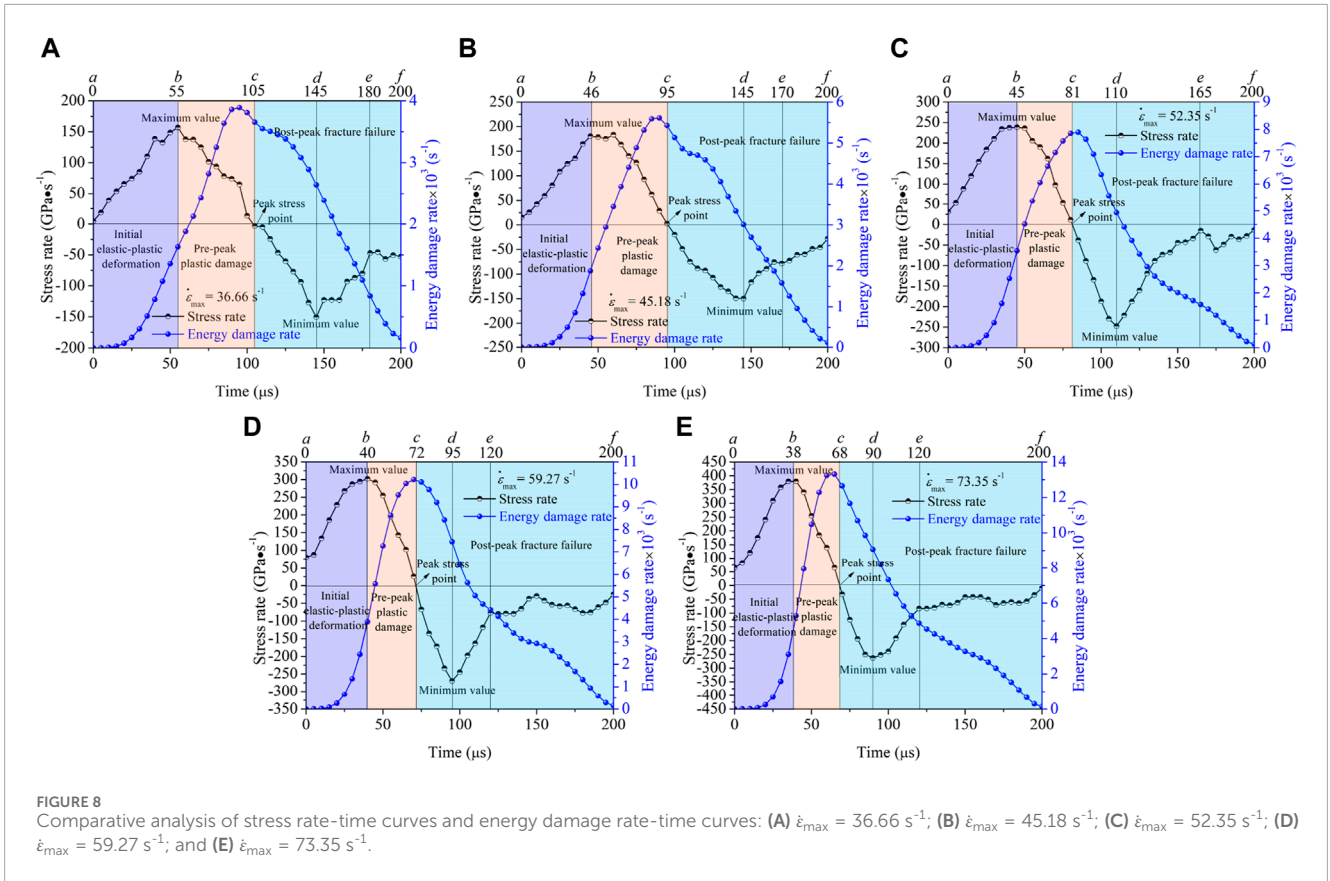
The stress wave propagation characteristics of RLM disks under impact splitting are shown in Figure 10. As shown in Figure 10A, both the reflected stress wave (σ_R) and the transmitted stress wave (σ_T) increased with the increase of the incident stress wave (σ_I), and the time for the transmitted stress wave to reach the peak value decreased with the increase of the incident stress wave, showing the advance effect of the transmitted stress peak value. As shown in Figure 10B, in the early stage (slight structural damage, 0–50 μs), the transmitted stress wave ratio (σ_T/σ_I) increased with the increase of strain rate, while in the later stage (large structural damage, 82–200 μs), the transmitted stress wave ratio (σ_T/σ_I) decreased with the increase of strain rate, which further indicated that the dynamic damage degree of RLM disks in the process of impact splitting affects the dynamic propagation coefficient of stress wave.

Based on the one-dimensional elastic stress wave propagation theory (Wang, 2007a; Wang, 2007b), the one-dimensional elastic stress wave propagation model of RLM disk under SHPB impact splitting can be further established (Figures 10C–E). It can be seen from Figures 10C–E that without considering the stress wave attenuation in the process of stress wave propagation, the one-dimensional elastic stress wave propagation characteristics of the RLM disk in the SHPB impact splitting process are mainly determined by the wave impedance (product of density and wave velocity) ratio and cross-sectional area ratio between different materials. As a result, the transmission stress ($\sigma_{T-2}^{1 \rightarrow 2}$) and reflection stress (σ_{R-1}) on the cross section-X12 at point B during the propagation of the one-dimensional elastic incident stress wave (σ_{I-1}) from the incident bar to the RLM disk under SHPB impact splitting can be further deduced (Eqs 4, 5):

$$\sigma_{T-2}^{1 \rightarrow 2} = \frac{2 \frac{A_1}{A_2}}{1 + \frac{\rho_1 C_1 A_1}{\rho_2 C_2 A_2}} \sigma_{I-1} \tag{4}$$

$$\sigma_{R-1} = \frac{1 - \frac{\rho_1 C_1 A_1}{\rho_2 C_2 A_2}}{1 + \frac{\rho_1 C_1 A_1}{\rho_2 C_2 A_2}} \sigma_{I-1} \tag{5}$$

Similarly, the transmission stress ($\sigma_{T-3}^{2 \rightarrow 3}$) and reflection stress (σ_{R-2}) on the cross section-X23 at point C during the propagation



of the one-dimensional elastic stress wave ($\sigma_{T-2} = \sigma_{T-2}^{1 \rightarrow 2}$) from the SHPB impact split RLM disk to the transmission bar can be further deduced (Eqs 6, 7):

$$\sigma_{T-3}^{2 \rightarrow 3} = \frac{2 \frac{A_2}{A_3}}{1 + \frac{\rho_2 C_2 A_2}{\rho_3 C_3 A_3}} \sigma_{T-2} \quad (6)$$

$$\sigma_{R-2} = \frac{1 - \frac{\rho_2 C_2 A_2}{\rho_3 C_3 A_3}}{1 + \frac{\rho_2 C_2 A_2}{\rho_3 C_3 A_3}} \sigma_{T-2} \quad (7)$$

According to Eq. 4 and Eqs 6, 7, the transmission stress ($\sigma_{T-3}^{1 \rightarrow 2 \rightarrow 3}$) and reflection stress (σ_{R-2}) on the cross section-X23 at point C during the propagation of the one-dimensional elastic incident stress wave (σ_{T-1}) from the incident bar to the transmission bar under SHPB impact splitting can be further deduced (Eqs 8, 9):

$$\sigma_{T-3}^{1 \rightarrow 2 \rightarrow 3} = \frac{2 \frac{A_1}{A_2} \times 2 \frac{A_2}{A_3}}{\left(1 + \frac{\rho_1 C_1 A_1}{\rho_2 C_2 A_2}\right) \left(1 + \frac{\rho_2 C_2 A_2}{\rho_3 C_3 A_3}\right)} \sigma_{T-1} \quad (8)$$

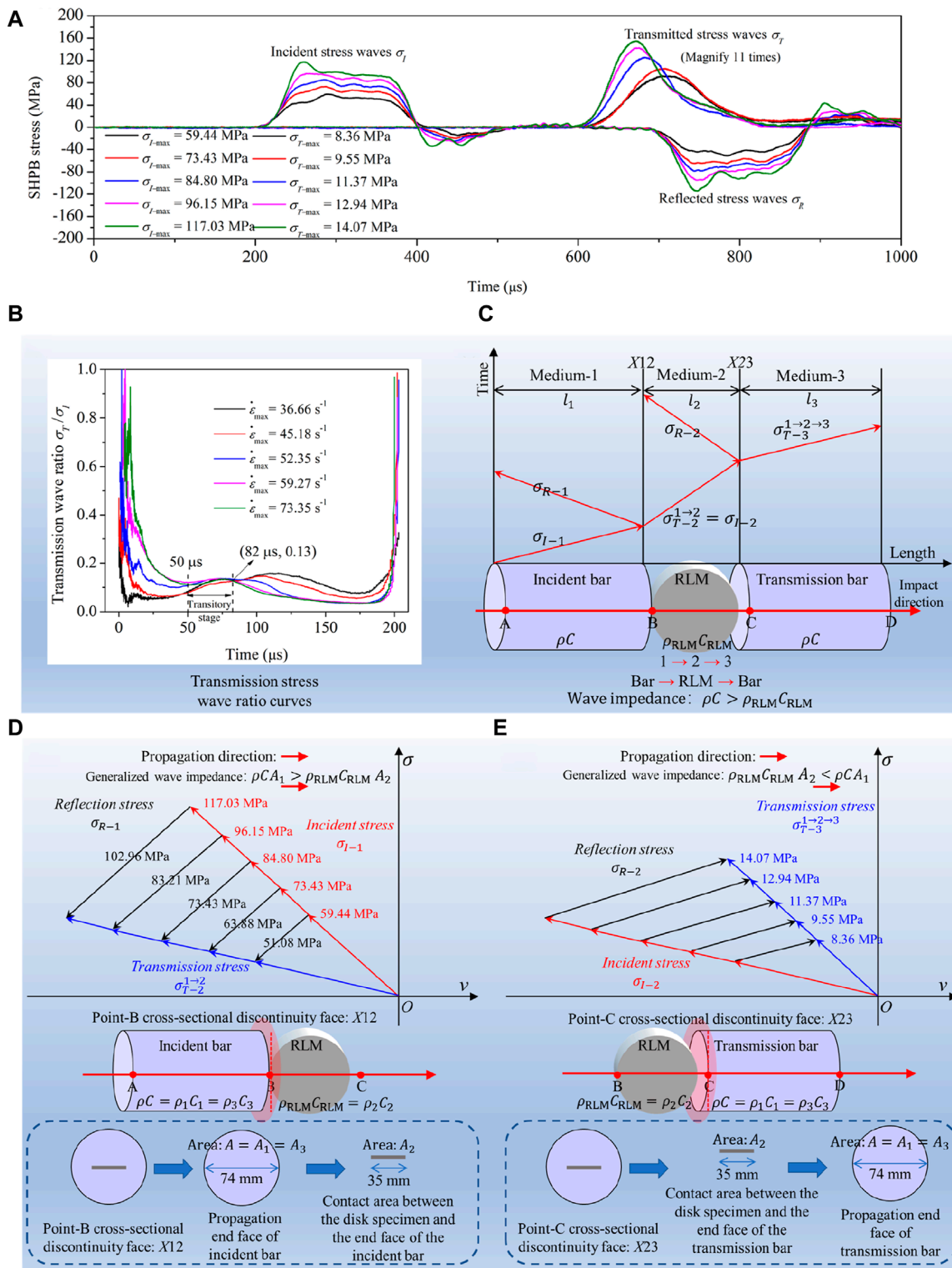
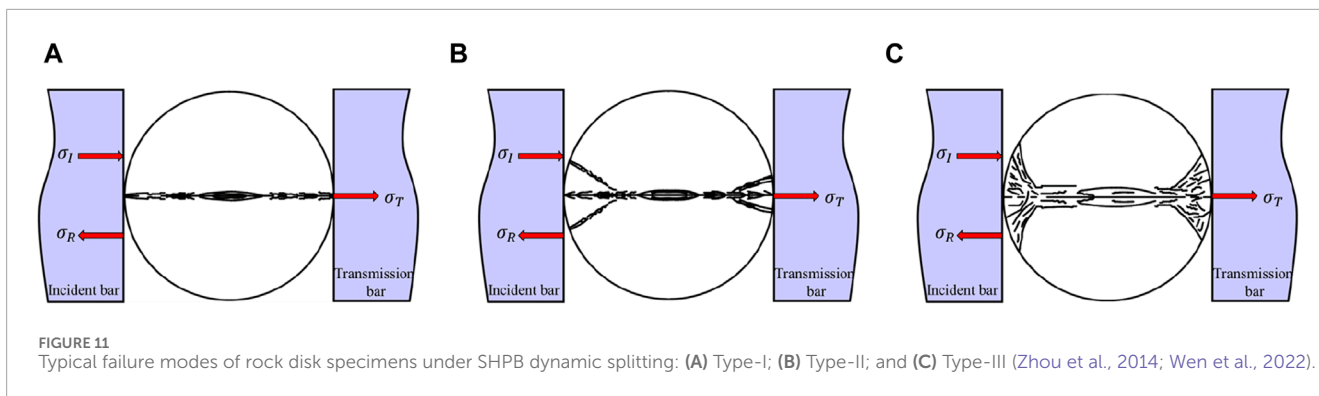


FIGURE 10 Stress wave propagation characteristics: (A) Typical SHPB three-stress wave-time curves; (B) stress wave propagation model; (C) transmission wave ratio-time curves; (D) reflection unloading; and (E) reflection loading.

$$\sigma_{R-2} = \frac{2 \frac{A_1}{A_2} \times \left(1 - \frac{\rho_2 C_2 A_2}{\rho_3 C_3 A_3}\right)}{\left(1 + \frac{\rho_1 C_1 A_1}{\rho_2 C_2 A_2}\right) \left(1 + \frac{\rho_2 C_2 A_2}{\rho_3 C_3 A_3}\right)} \sigma_{I-1} \quad (9)$$

where: A_1 and A_2 are the cross sectional areas of the incident bar (medium-1) and the transmission bar (medium-3); A_3 is the contact area between the rock sample (medium-2) and the incident bar and the transmission bar; ρ_1 , ρ_2 , and ρ_3 are the densities of



medium-1, medium-2, and medium-3, respectively, C_1 , C_2 , and C_3 are the longitudinal wave velocities of medium-1, medium-2, and medium-3, respectively.

5 Discussion

The damage and failure characteristics of rock specimens under external load are the final form of the evolution of internal micro-cracks, which makes the failure characteristics of rock specimens contain key information such as deformation law, stress distribution, and crack propagation (Wen et al., 2022). Therefore, the analysis of the dynamic failure characteristics of rock specimens is of great significance to reveal the dynamic failure mechanism of rock mass. In terms of failure characteristics, typical related studies are as follows: based on the SHPB dynamic splitting test of granite, Zhou et al. (2014) divided the splitting failure modes of granite disk specimens into three types: “axial splitting under central initiation (type-I)”, “end wedge-shaped failure + axial splitting under central initiation (type-II)” and “end wedge-shaped failure + middle axial fracture zone under end initiation (type-III)”, as shown in Figure 11. In terms of failure mechanism, for the reason that there is a great difference between the type-III fracture mode and the standard Brazilian splitting failure mode, Zhou et al. (2014) thought that the impact velocity of the incident bar increases the friction between the bar and the specimen, and the local friction affects the stress distribution of the specimen, which leads to premature damage of the bar-specimen contact area (the loading end of the specimen), which further affects the stress distribution and deformation ability of the specimen. Xue et al. (2013) thought that it may be because there is damage or the structural weak surface at the loading end of the specimen before loading, which leads to the damage first when it is subjected to dynamic loading, so the dynamic Brazilian splitting does not necessarily start from the center, and the location of the crack is closely related to the structural state of the specimen itself.

In addition, in terms of failure characteristics, Yang et al. (2023) through the SHPB dynamic splitting test and numerical simulation of sandstone and RLM found that semicircle bending fracture failure occurred in sandstone and RLM specimens under large impact load. Su et al. (2023) also found the phenomenon of semicircle bending fracture failure through SHPB dynamic splitting test and numerical

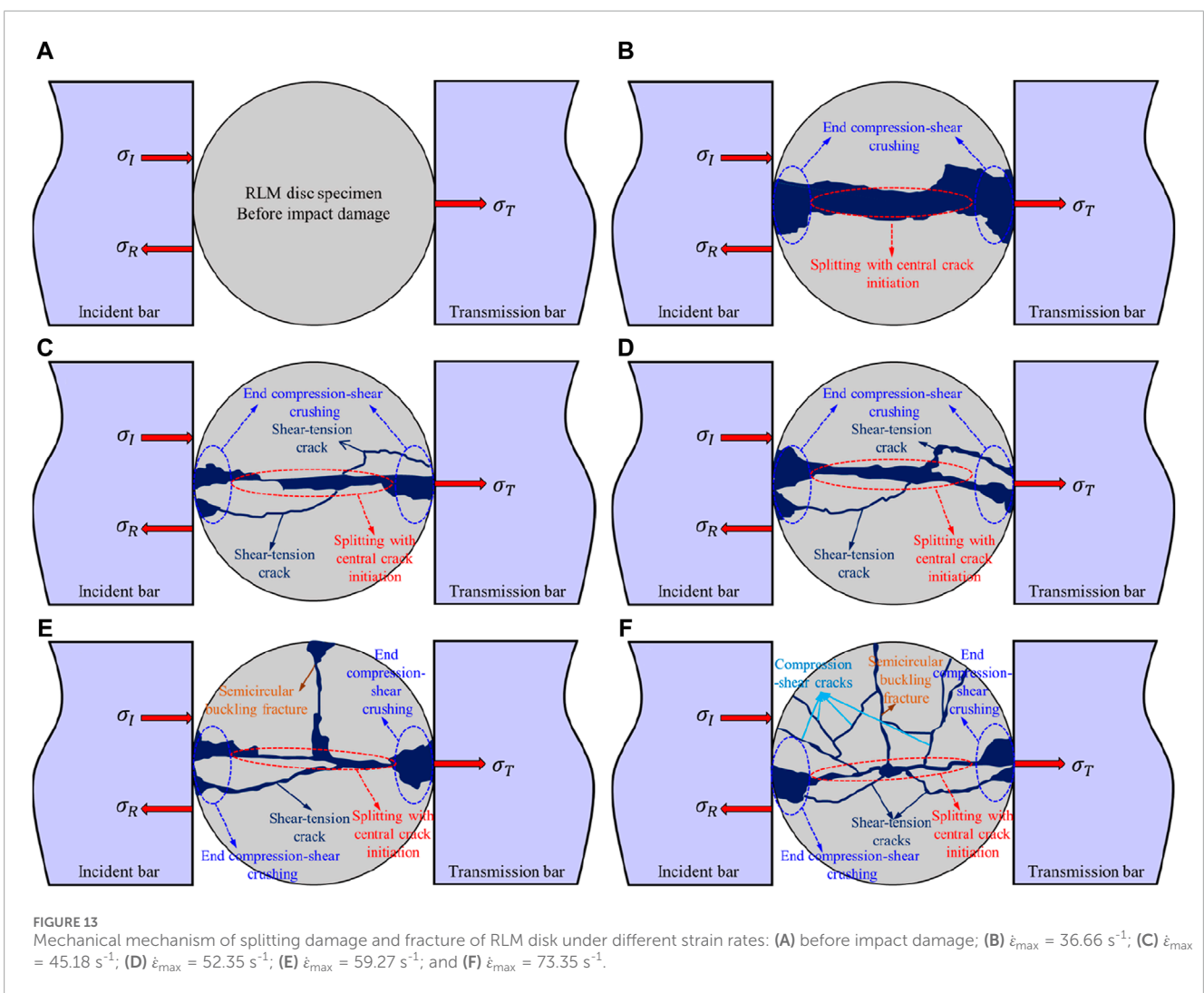
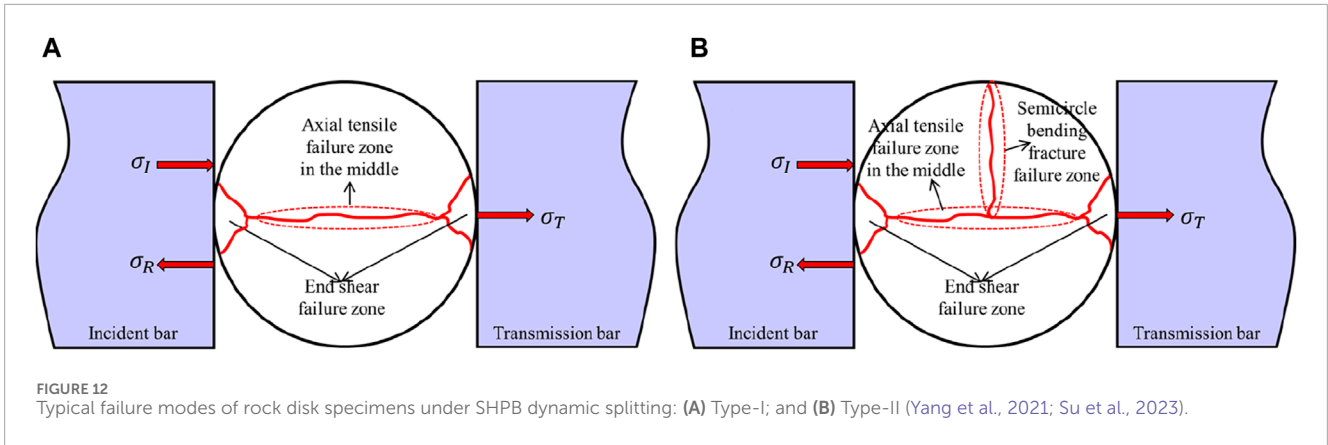
simulation of frozen sandstone, and divided the failure modes into two types: “end triangular shear failure + middle axial tensile failure (type-I)” and end triangular shear failure + middle axial tensile failure + semicircle bending fracture (type-II), as shown in Figure 12. Wang et al. (2020) also found the phenomenon of semicircle bending fracture through the SHPB dynamic splitting test of heat-treated sandstone. In terms of failure mechanism, Yang et al. (2023, 2021) considered that after the splitting tensile fracture of the disk specimen was completed, the damage at the loading end of the specimen further increased with the continued action of a larger external force, and bending cracks were formed at the upper or lower end of the semicircle specimen due to stress concentration in about the vertical loading direction, and finally formed a semicircle bending fracture. However, the above research does not deeply reveal the damage mechanism of rock disk specimens under SHPB impact splitting.

To sum up, compared with the static Brazil splitting test, the SHPB dynamic Brazil splitting test is likely to show a more complex damage mode which is different from the static Brazil splitting test due to many factors such as strain rate effect and stress wave propagation. For this test, from the damage modes of RLM disks under SHPB impact splitting, RLM disks actually contain the damage and fracture mechanics mechanism that needs to be further revealed under SHPB impact splitting. According to the actual damage characteristics of RLM disks under SHPB impact splitting, the clearer damage mode diagrams can be obtained (Figure 13). As can be seen from Figure 13, with the increase of strain rate, the macro-damage failure modes of RLM disks mainly developed in the direction of “end compression-shear failure + middle axial splitting” → “end compression-shear failure + middle axial splitting + semicircle shear-tension fracture” → “end compression-shear failure + middle axial splitting + semicircle shear-tension fracture + semicircle bending fracture”.

The damage and failure mode of rock material is the external reflection of its internal damage and failure mechanism (Wang J. et al., 2022). To deeply reveal the damage and failure mechanism contained in the damage and failure modes of RLM disks under SHPB impact splitting, the damage and failure mechanisms of the following two aspects were analyzed from the point of view with mechanics.

(1) End compression-shear fracture mechanism

In the process of dynamic loading, the center of the disk specimen is in a state of tensile stress concentration, which causes the



tensile crack to first occur from the center of the specimen (central crack initiation) and rapidly expand along the axial loading direction to the two loading ends of the specimen, and finally form a tensile fracture, and the specimen is split into two-halves (Yang et al., 2020). In this process, the two loading ends of the specimen are also in a

state of compression stress concentration due to mutual extrusion with the bars, resulting in compression damage at the two loading ends of the specimen. However, with the continuous action of impact load, the loading ends of the specimen change from compression stress concentration to compression-shear stress concentration, and

then form a wedge-shaped compression-shear fracture zone at the two loading ends.

- (2) Shear-tension crack formation mechanism and semicircle bending fracture mechanism

In the process of the disk specimen splitting to form two semicircles, because the tensile strain of the disk specimen decreases from the center to both ends along the loading direction, the specimen is subjected to bending and shear under the extrusion of the bars (Yang et al., 2020). After the tensile failure of the specimen, the bending and shear of the two semicircle specimens are more obvious with the continued action of the impact load. According to the stability theory of compression bars, the two semicircle specimens are essentially in a state of stress concentration in shear-tension at the end and buckling in the middle. Therefore, under the continuous action of a larger impact load, the shear-tension cracks will occur at the end of the two semicircle specimens along the loading direction. Further, the semicircle bending fracture of the two semicircle specimens will also occur in the vertical loading direction. It is worth noting that the upper semicircle is more prone to buckling fracture than the lower semicircle, which may be due to the fact that it is relatively difficult for the upper semicircle to escape from the continued action of SHPB under the action of dead weight.

6 Conclusion

In this work, the meso-damage mechanical behavior and stress wave propagation characteristics of RLM disks under impact splitting were studied by using large-diameter SHPB, and the dynamic mechanical mechanism of splitting damage and fracture of RLM disks under different strain rates is discussed deeply. The following conclusions were drawn.

- (1) The splitting tensile stress-compression strain curves of RLM disks obviously showed three stages of mechanical behavior evolution: initial elastic-plastic deformation, pre-peak plastic damage and post-peak brittle fracture failure. The tensile fracture of RLM disks at meso-level was the result of both initial meso-damage and impact splitting meso-damage.
- (2) The dynamic splitting damage variable defined based on the damage fracture energy accurately described the evolution characteristics of impact splitting damage of RLM disks, and the impact splitting strength depended on the degree of dynamic splitting damage.
- (3) The time for the transmission stress wave to reach the peak value decreased with the increase of the incident stress wave, which showed the advance effect of the transmission stress peak value, and the dynamic damage degree in the impact splitting process affected the dynamic propagation coefficient of the stress wave.
- (4) The propagation characteristics of one-dimensional elastic stress waves in the process of impact splitting are mainly determined by the wave impedance ratio and cross-sectional area ratio of different materials. The stress wave propagation model based on one-dimensional elastic stress wave theory clearly revealed the stress wave propagation law in the process of impact splitting of RLM disks.

- (5) With the increase of strain rate, the damage modes of RLM disks mainly developed in the direction of “end compression-shear failure + middle axial splitting” → “end compression-shear failure + middle axial splitting + semicircle shear-tension fracture” → “end compression-shear failure + middle axial splitting + semicircle shear-tension fracture + semicircle bending fracture”, and the upper semicircle was more prone to buckling fracture than the lower semicircle.

Data availability statement

The original contributions presented in the study are included in the article/supplementary material, further inquiries can be directed to the corresponding authors.

Author contributions

RY: Conceptualization, Data curation, Formal Analysis, Funding acquisition, Investigation, Methodology, Project administration, Visualization, Writing–original draft, Writing–review and editing. YX: Conceptualization, Funding acquisition, Methodology, Resources, Supervision, Writing–review and editing. MY: Investigation, Writing–review and editing. JG: Investigation, Writing–review and editing. QA: Investigation, Writing–review and editing. PM: Funding acquisition, Investigation, Writing–review and editing.

Funding

The author(s) declare that financial support was received for the research, authorship, and/or publication of this article. The authors gratefully acknowledge the financial support from the Natural Science Research Project of Anhui Educational Committee (2023AH051167), Scientific Research Foundation for High-level Talents of Anhui University of Science and Technology (2022yjrc84), Sub-project of National Key R & D Program (2021YFB3401504), National Natural Science Foundation of China (52074009, 52274071), and the Innovation and Entrepreneurship Training Program for College Students in Anhui Province (S202310361228).

Conflict of interest

Author RY was employed by Anhui Hongchang New Materials Co., Ltd.

The remaining authors declare that the research was conducted in the absence of any commercial or financial relationships that could be construed as a potential conflict of interest.

Publisher's note

All claims expressed in this article are solely those of the authors and do not necessarily represent those of their affiliated organizations, or those of the publisher, the editors and the reviewers. Any product that may be evaluated in this article, or claim that may be made by its manufacturer, is not guaranteed or endorsed by the publisher.

References

- Ai, D., Zhao, Y., Wang, Q., and Li, C. (2019). Experimental and numerical investigation of crack propagation and dynamic properties of rock in SHPB indirect tension test. *Int. J. Impact Eng.* 126, 135–146. doi:10.1016/j.ijimpeng.2019.01.001
- Chen, S., Zhang, H., Wang, L., Yuan, C., Meng, X., Yang, G., et al. (2022). Experimental study on the impact disturbance damage of weakly cemented rock based on fractal characteristics and energy dissipation regulation. *Theor. Appl. Fract. Mech.* 122, 103665. doi:10.1016/j.tafmec.2022.103665
- Chen, X., Li, L., Wang, L., and Qi, L. (2019). The current situation and prevention and control countermeasures for typical dynamic disasters in kilometer-deep mines in China. *Saf. Sci.* 115, 229–236. doi:10.1016/j.ssci.2019.02.010
- Deng, J., Kanwar, N. S., Pandey, M. D., and Xie, W. C. (2019). Dynamic buckling mechanism of pillar rockbursts induced by stress waves. *J. Rock Mech. Geotechnical Eng.* 11 (5), 944–953. doi:10.1016/j.jrmge.2019.02.005
- Fairhurst, C. (2017). Some challenges of deep mining. *Engineering* 3 (4), 527–537. doi:10.1016/j.ENG.2017.04.017
- Gao, Q., Zhang, Q., Zhang, X., and Zhang, L. (2018). Geomechanical model test and energy mechanism analysis of zonal disintegration in deep surrounding rock. *Geosciences* 8 (7), 237. doi:10.3390/geosciences8070237
- Guo, Li., Chen, Q., Wu, Y., Zhang, Q., and Qi, C. (2022). Numerical simulation of adjacent stope interaction and parametric analysis of the creep behavior of rock mass. *J. Mater. Res. Technol.* 19, 2063–2076. doi:10.1016/j.jmrt.2022.05.112
- Guo, Z., and Man, K. (2022). Experimental and mechanism of granite on its dynamic splitting tensile property. *Sci. Technol. Eng.* 22 (6), 2177–2184.
- Han, Z., Li, D., and Li, X. (2022). Dynamic mechanical properties and wave propagation of composite rock-mortar specimens based on SHPB tests. *Int. J. Min. Sci. Technol.* 32 (4), 793–806. doi:10.1016/j.ijmst.2022.05.008
- Hu, X., Su, G., Li, Z., Xu, C., Yan, X., Liu, Y., et al. (2021). Suppressing rockburst by increasing the tensile strength of rock surface: an experimental study. *Tunn. Undergr. Space Technol.* 107, 103645. doi:10.1016/j.tust.2020.103645
- Le, H., Sun, S., and Wei, J. (2019). Influence of types of grouting materials on compressive strength and crack behavior of rocklike specimens with single grout-infilled flaw under axial loads. *J. Mater. Civ. Eng.* 31 (1), 06018022. doi:10.1061/(ASCE)MT.1943-5533.0002554
- Li, C. C., Zhao, T., Zhang, Y., and Wan, W. (2020). A study on the energy sources and the role of the surrounding rock mass in strain burst. *Int. J. Rock Mech. Min. Sci.* 154, 105114. doi:10.1016/j.ijrmms.2022.105114
- Li, L., Wang, M., Fan, P., Jiang, H., Cheng, Y., and Wang, D. (2016). Strain rockbursts simulated by low-strength brittle equivalent materials. *Adv. Mater. Sci. Eng.* 2016, 1–11. doi:10.1155/2016/5341904
- Li, P., Cai, M., Gao, Y., Wang, P., Miao, S., Wang, Y., et al. (2023a). Dynamic mechanical behavior and cracking mechanism of cross-jointed granite containing a hole. *J. Mater. Res. Technol.* 22, 1572–1594. doi:10.1016/j.jmrt.2022.12.034
- Li, X., Gao, W., Guo, L., Li, Z., and Zhang, S. (2023b). Influences of the number of non-consecutive joints on the dynamic mechanical properties and failure characteristics of a rock-like material. *Eng. Fail. Anal.* 146, 107101. doi:10.1016/j.engfailanal.2023.107101
- Liu, X., Song, S., Tan, Y., Fan, D., Ning, J., Li, X., et al. (2021). Similar simulation study on the deformation and failure of surrounding rock of a large section chamber group under dynamic loading. *Int. J. Min. Sci. Technol.* 31 (3), 495–505. doi:10.1016/j.ijmst.2021.03.009
- Ma, T. H., Tang, C. A., Tang, L. X., Zhang, W. D., and Wang, L. (2015). Rockburst characteristics and microseismic monitoring of deep-buried tunnels for Jinping II Hydropower Station. *Tunn. Undergr. Space Technol.* 49, 345–368. doi:10.1016/j.tust.2015.04.016
- Ren, Y., Sun, Y., and Meng, X. (2023). Multi-scale structural characteristics and the damage evolution mechanism of rock under load. *Mater. Lett.* 331, 133430. doi:10.1016/j.matlet.2022.133430
- Su, H., Zhu, Z., and Wang, L. (2023). Experimental and numerical analysis of dynamic splitting mechanical properties and crack propagation for frozen sandstone. *Int. J. Rock Mech. Min. Sci.* 163, 105325. doi:10.1016/j.ijrmms.2022.105325
- Toi, Y., and Kiyosue, T. (1995). Damage mechanics models for brittle microcracking solids based on three-dimensional mesoscopic simulations. *Eng. Fract. Mech.* 50 (1), 11–27. doi:10.1016/0013-7944(94)00160-j
- Wang, J., Ma, L., Zhao, F., Lv, B., Gong, W., He, M., et al. (2022). Dynamic strain field for granite specimen under SHPB impact tests based on stress wave propagation. *Undergr. Space* 7 (5), 767–785. doi:10.1016/j.undsp.2021.11.010
- Wang, L.-L. (2007a). Elementary theory of one-dimensional stress waves in bars. *Found. Stress Waves*, 7–55. doi:10.1016/B978-008044494-9/50002-0
- Wang, L.-L. (2007b). Interaction of elastic longitudinal waves. *Found. Stress Waves*, 57–93. doi:10.1016/B978-008044494-9/50003-2
- Wang, P., Yin, T., and Hu, B. (2020). Dynamic tensile strength and failure mechanisms of thermally treated sandstone under dry and water-saturated conditions. *Trans. Nonferrous Metals Soc. China* 30 (8), 2217–2238. doi:10.1016/S1003-6326(20)65374-2
- Wang, Q. Z., Li, W., and Xie, H. P. (2009). Dynamic split tensile test of Flattened Brazilian Disc of rock with SHPB setup. *Mech. Mater.* 41 (3), 252–260. doi:10.1016/j.mechmat.2008.10.004
- Wang, Y., Tang, P., Han, J., and Li, P. (2023). Energy-driven fracture and instability of deeply buried rock under triaxial alternative fatigue loads and multistage unloading conditions: prior fatigue damage effect. *Int. J. Fatigue* 168, 107410. doi:10.1016/j.ijfatigue.2022.107410
- Wang, Z., Wang, M., Zhou, L., Zhu, Z., Shu, Y., and Peng, T. (2022). Research on uniaxial compression strength and failure properties of stratified rock mass. *Theor. Appl. Fract. Mech.* 121, 103499. doi:10.1016/j.tafmec.2022.103499
- Wen, X., Feng, G., Guo, J., Wang, P., Qian, R., Zhu, L., et al. (2022). Dynamic tensile mechanical response properties of sandstone under medium and low strain rate disturbance load. *Chin. J. Rock Mech. Eng.* 41 (S1), 2812–2822. doi:10.13722/j.cnki.jrme.2021.0691
- Wu, Q., Li, X., Weng, L., Li, Q., Zhu, Y., and Luo, R. (2019). Experimental investigation of the dynamic response of prestressed rockbolt by using an SHPB-based rockbolt test system. *Tunn. Undergr. Space Technol.* 93, 103088. doi:10.1016/j.tust.2019.103088
- Xia, K., Wang, S., Xu, Y., Chen, R., and Wu, B. (2021). Advances in experimental studies for deep rock dynamics. *Chin. J. Rock Mech. Eng.* 40 (3), 448–475. doi:10.13722/j.cnki.jrme.2020.0343
- Xia, K., Xu, Y., and Chen, R. (2019). Dynamic tests of rocks subjected to simulated deep underground environments. *Hazard Control Tunn. Undergr. Eng.* 1 (1), 58–75.
- Xia, K., and Yao, W. (2015). Dynamic rock tests using split Hopkinson (Kolsky) bar system - a review. *J. Rock Mech. Geotechnical Eng.* 7 (1), 27–59. doi:10.1016/j.jrmge.2014.07.008
- Xie, H., Lu, J., Li, C., Li, M., and Gao, M. (2022). Experimental study on the mechanical and failure behaviors of deep rock subjected to true triaxial stress: a review. *Int. J. Min. Sci. Technol.* 32 (5), 915–950. doi:10.1016/j.ijmst.2022.05.006
- Xue, R., Liang, Z., and Xu, N. (2021). Rockburst prediction and analysis of activity characteristics within surrounding rock based on microseismic monitoring and numerical simulation. *Int. J. Rock Mech. Min. Sci.* 142, 104750. doi:10.1016/j.ijrmms.2021.104750
- Xue, Y., Liu, T., Tang, L., Dong, L., and Zhang, J. (2013). Study of SHPB dynamic split crack initiation and propagation. *J. Wuhan Univ. Technol.* 35 (3), 97–101. doi:10.3963/j.issn.1671-4431.2013.03.020
- Yang, F., Zhou, H., Xiao, H., Azhar, M. U., Zhu, Y., and Chi, F. (2022). Numerical simulation method for the process of rockburst. *Eng. Geol.* 306, 106760. doi:10.1016/j.enggeo.2022.106760
- Yang, R., Li, W., Li, Y., Fang, S., and Zhu, Y. (2020). Comparative analysis on dynamic tensile mechanical properties of three kinds of rocks. *J. China Coal Soc.* 45 (9), 3107–3118. doi:10.13225/j.cnki.jccs.2019.0853
- Yang, R., Xu, Y., Chen, P., and Wang, J. (2021). Experimental study on dynamic mechanics, energy characteristics, and failure mechanism of rubber cement mortar under SHPB splitting test. *Mater. Rep.* 35 (10), 10062–10072. doi:10.11896/cldb.20030105
- Yang, R., Xu, Y., Liu, J., Ding, J., and Xie, H. (2023). Comparative analysis of dynamic mechanics and failure characteristics of sandstone and quasi-sandstone material. *Mater. Rep.* 37 (23), 70–80. doi:10.11896/cldb.22030265
- Yuan, X. P., Liu, H. Y., and Wang, Z. Q. (2013). An interacting crack-mechanics based model for elastoplastic damage model of rock-like materials under compression. *Int. J. Rock Mech. Min. Sci.* 58, 92–102. doi:10.1016/j.ijrmms.2012.09.007
- Zhai, S., Su, G., Yin, S., Zhao, B., and Yan, L. (2020). Rockburst characteristics of several hard brittle rocks: a true triaxial experimental study. *J. Rock Mech. Geotechnical Eng.* 12 (2), 279–296. doi:10.1016/j.jrmge.2019.07.013
- Zhang, F., Peng, J., Qiu, Z., Chen, Q., Li, Y., and Liu, J. (2017). Rock-like brittle material fragmentation under coupled static stress and spherical charge explosion. *Eng. Geol.* 220, 266–273. doi:10.1016/j.enggeo.2017.02.016
- Zhang, Q., Li, F., Duan, K., Yu, G., Cheng, L., and Guo, X. (2021). Experimental investigation on splitting failure of high sidewall cavern under three-dimensional high in-situ stress. *Tunn. Undergr. Space Technol.* 108, 103725. doi:10.1016/j.tust.2020.103725
- Zheng, Y., Shan, R., Huang, B., Feng, J., and Peng, R. (2021). Similar model tests on strong sidewall and corner support of gob side entry retaining. *J. Min. Saf. Eng.* 38 (1), 94–102. doi:10.13545/j.cnki.jmse.2019.0491
- Zhou, Z., Li, X., Zou, Y., Jiang, Y., and Li, G. (2014). Dynamic brazilian tests of granite under coupled static and dynamic loads. *Rock Mech. Rock Eng.* 47, 495–505. doi:10.1007/s00603-013-0441-4
- Zhu, Q., Li, T., Zhang, H., Ran, J., Li, H., Du, Y., et al. (2022). True 3D geomechanical model test for research on rheological deformation and failure characteristics of deep soft rock roadways. *Tunn. Undergr. Space Technol.* 128, 104653. doi:10.1016/j.tust.2022.104653
- Zuo, Y., Ma, C., Zhu, W., Li, S., Gong, F., and Chen, C. (2011). Model test study of mechanism of layered fracture within surrounding rock of tunnels in deep stratum tunnelling under dynamic disturbance. *Rock Soil Mech.* 32 (10), 2929–2936. doi:10.16285/j.rsm.2011.10.009